ADVANCES IN ATMOSPHERIC SCIENCES, VOL. 35, DECEMBER 2018, 1547–1552

• **Original Paper** •

A Limb Correction Method for the Microwave Temperature Sounder 2 and Its Applications

Xiaoxu TIAN[1], Xiaolei ZOU*[1], and Shengpeng YANG[2]

[1]*Earth Science System Interdisciplinary Center, University of Maryland, College Park, Maryland* 20740*, USA*
[2]*Joint Center for Data Assimilation Research and Applications, Nanjing University of Information Science and Technology, Nanjing* 210042*, China*

(Received 18 April 2018; revised 14 June 2018; accepted 5 July 2018)

ABSTRACT

The Microwave Temperature Sounder 2 (MWTS-2) is a cross-track radiometer that has 13 channels of sampling radiances emitted from different vertical levels of the atmosphere. Because of the varying scan angles of each field of view within a scan line, observations from the MWTS-2 are subject to strong scan-position-dependent features, i.e., the limb effect. When examining brightness temperatures (TBs), weather signals observed at every temperature-sounding channel are often concealed by scan-dependent patterns. This study, therefore, proposes a limb correction method to remove scan-dependent features so that the underlying weather signals can be uncovered. Limb-corrected TBs can be used to monitor large-scale patterns over the globe as well as extreme weather events such as typhoons. Limb-corrected TBs are also more correlated with atmospheric physical variables such as temperature and liquid water path.

Key words: MWTS-2, Limb Correction, Tropical cyclones, weather monitoring

Citation: Tian, X., X. Zou, and S. Yang, 2018: A limb correction method for the Microwave Temperature Sounder 2 and its applications. *Adv. Atmos. Sci.*, **35**(12), 1547–1552, https://doi.org/10.1007/s00376-018-8092-8.

1. Introduction

The Microwave Temperature Sounder 2 (MWTS-2) is onboard the FengYun 3C satellite that was successfully launched into a sun-synchronous orbit with an equator crossing time of 1015 LST (descending node). The MWTS-2 has a total of 13 channels, all of which are temperature-sounding channels with peak weighting functions ranging from the lower troposphere to the upper stratosphere (Wang and Li, 2014; Li et al., 2016). The swath width is 2250 km, with 90 fields of view (FOVs) in one scan line. Microwave temperature sounders such as the MWTS-2 are critical instruments used to monitor weather around the globe. Unlike infrared instruments, microwave radiances can penetrate non-precipitating clouds, making it possible to obtain weather information beneath clouds. Zou et al. (2013) found positive impacts on hurricane track and intensity forecasts by assimilating Advanced Technology Microwave Sounder (ATMS) radiances into the Hurricane Weather Research and Forecasting model. Tian and Zou (2016) retrieved internal three-dimensional thermal structures using observations from the Advanced Microwave Sounding Unit-A (AMSU-A) and ATMS. The algorithm was further applied to devastating hurricane cases such as Hurricanes Harvey, Irma, and Maria of 2017 (Tian and Zou, 2018). Li and Liu (2016) demonstrated that assimilating MWTS radiances over the Northern Hemisphere into the Global and Regional Assimilation and Prediction System had a positive impact on weather forecasts.

Because the MWTS-2 is a cross-track radiometer, radiances are observed at different scan angles within a scan line. As a result, brightness temperatures (TBs) at every channel are primarily associated with scan-dependent features. A greater scan angle (i.e., farther from nadir) generally implies a longer optical path, resulting in an elevated weighting function compared with that at nadir. TBs are colder at FOV positions with large scan angles in the troposphere, where temperatures decrease as the altitude increases. Similarly, in the stratosphere, where temperatures increase with increasing altitude, observed TBs tend to be warmer off-nadir than at nadir. Weather signals in the atmosphere are thus difficult to discern by direct examination of MWTS-2 observations. Goldberg et al. (2001) proposed a limb effect adjustment algorithm for the AMSU-A. AMSU-A measurements after the limb effect adjustment became statistically similar at all scan angles. Zhang et al. (2017) applied the algorithm proposed by Goldberg et al. (2001) to ATMS observations. This study presents a limb effect correction algorithm for the MWTS-2. TBs before and after limb correction are compared to show the weather signals revealed by the limb-corrected (LC) TBs.

* Corresponding author: Xiaolei ZOU
Email: xzou1@umd.edu

2. MWTS-2 limb correction algorithm description

A given channel and its neighboring channels whose weighting functions peak immediately above and/or below are used as the predictors when calculating scan-dependent patterns for most channels. Table 1 lists the predictors for each channel and the peak weighting function pressure levels. The limb correction coefficient training equation is defined as

$$\overline{T_{k,\mathrm{nadir}}}(j_2) = b_i + \sum_{k_\mathrm{p}=k-1}^{k=1} a_{k_\mathrm{p},i}[T_{k_\mathrm{p}}(i,j_2) - \overline{T_{k_\mathrm{p}}(i)}]\,, \qquad (1)$$

where $\overline{T_{k,\mathrm{nadir}}}(j_2)$ is the mean TB (units: K) at channel k of FOV positions 45 and 46 estimated in every 2° latitudinal band Wark (1993), and j_2 is the index for every 2° latitudinal band. The variable $T_{k_\mathrm{p}}(i,j_2)$ is the mean TB at the predictor channel k_p of FOV position i, also estimated at every 2° latitudinal band, while $\overline{T_{k_\mathrm{p}}(i)}$ is estimated globally. The coefficients $a_{k_\mathrm{p},i}$ and b_i are regression coefficients to be trained. These coefficients and $\overline{T_{k_\mathrm{p}}(i)}$ are stored for use in calculating LC TBs. After the coefficients are obtained, the LC TB can be written as

$$T_{k,\mathrm{LC}}(i,j) = b_i + \sum_{k_\mathrm{p}=k-1}^{k+1} a_{k_\mathrm{p},i}[T_{k_\mathrm{p}}(i,j) - \overline{T_{k_\mathrm{p}}(i)}]\,, \qquad (2)$$

where $T_{k,\mathrm{LC}}(i,j)$ represents the LC TB of channel k at FOV position i and scan line j. For channels 1 to 5, only observations over oceans are included in the calculations. For channels 6 to 13, no surface type separations are made. Figure 1

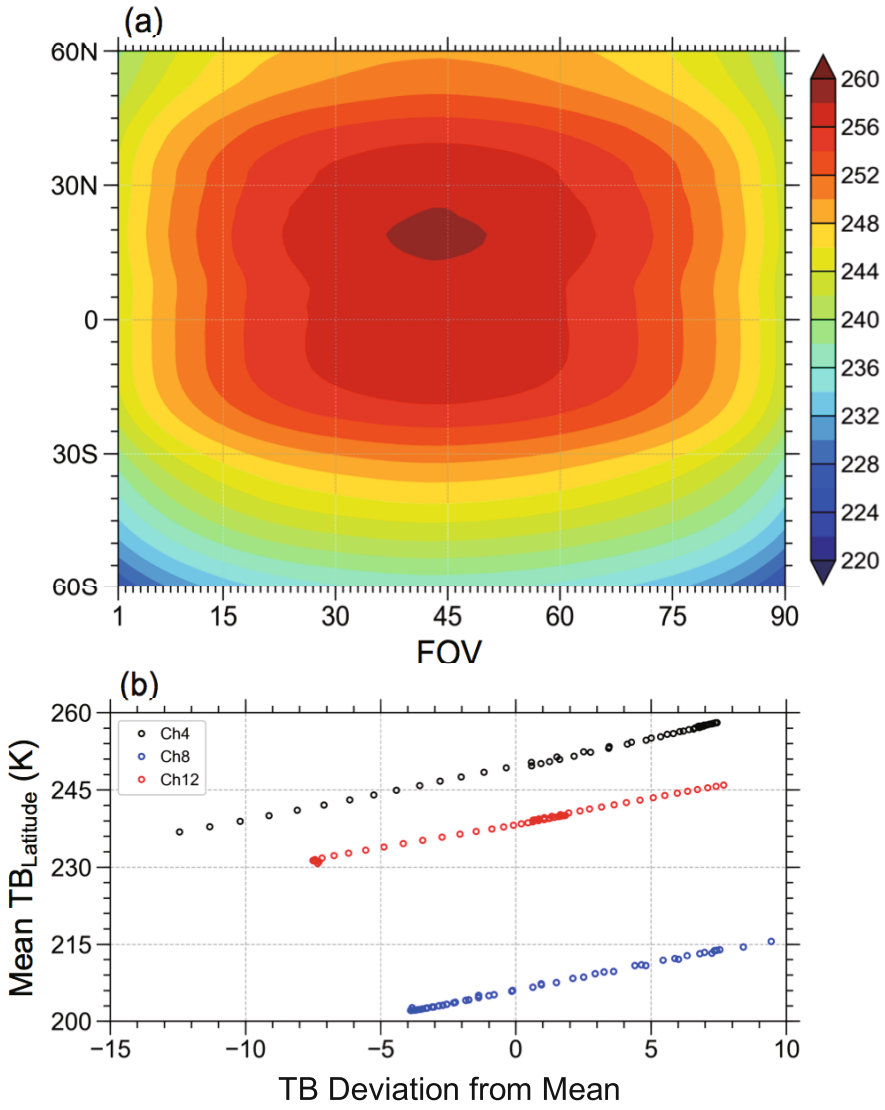

Fig. 1. (a) MWTS-2 channel 4 mean TBs (units: K) averaged at every scan position and in every 2° latitudinal band. Data are from July 2014. (b) Mean nadir TBs estimated in every 2° latitudinal band as a function of the differences between the latitudinal averages in (a) and globally averaged TBs at each scan position for channels 4 (black circles), 8 (blue circles), and 12 (red circles).

Table 1. Predictor channels and peak weighting functions of the 13 MWTS-2 channels.

Frequency (GHz)	Channel	Predictor channels	Peak WF (hPa)
50.3	1	1, 2, 3	Surface
51.76	2	1, 2, 3	Surface
52.8	3	2, 3, 4	1,000
53.596	4	3, 4, 5	700
54.4	5	4, 5, 6	400
54.94	6	5, 6	270
55.5	7	7, 8, 9	180
$f_0 = 57.29$	8	8, 9	90
$f_0 \pm 0.217$	9	8, 9, 10	50
$f_0 \pm 0.322 \pm 0.048$	10	9, 10, 11	25
$f_0 \pm 0.322 \pm 0.022$	11	10, 11	12
$f_0 \pm 0.322 \pm 0.01$	12	10, 11, 12	5
$f_0 \pm 0.322 \pm 0.0045$	13	12, 13	2

shows mean channel 4 TBs averaged over every 2° latitudinal band, i.e., $T_{k_p}(i, j_2)$ in the two previous equations, and the relationship between the mean nadir TB in every 2° latitudinal band $[T_{k,\text{nadir}}(j_2)]$ with respect to $T_{k_p}(i, j_2) - \overline{T_{k_p}(i)}$ at channels 3 and 4. A tight linear relationship exists between these two quantities.

3. Limb-Corrected Brightness Temperatures

The regression coefficients were trained with mean MWTS-2-derived TBs from every 2° latitudinal band in July 2014. Figure 2 shows channel 4 TBs before and after limb correction over the globe on 7 July 2014. Only the dominant scan patterns can be seen within each swath before limb correction (Fig. 2a). The temperature field after limb correction, by contrast, begins to reflect large-scale atmospheric weather features (Fig. 2b). The limb-corrected TBs at the conjunction of two neighboring swaths are coherent. This coherence is physically realistic because the MWTS-2 is sampling a globally continuous temperature field in separate swaths that are about 100 min apart. Magnification of the western Pacific Ocean shows that Category 5 Typhoon Neoguri is covered by one of the MWTS-2 swaths (Figs. 3a and b). Before limb correction (Fig. 3a), a cyclone-shaped feature can be seen under the predominant scan patterns. Typhoon Neoguri's characteristics are seen more clearly after limb correction, including

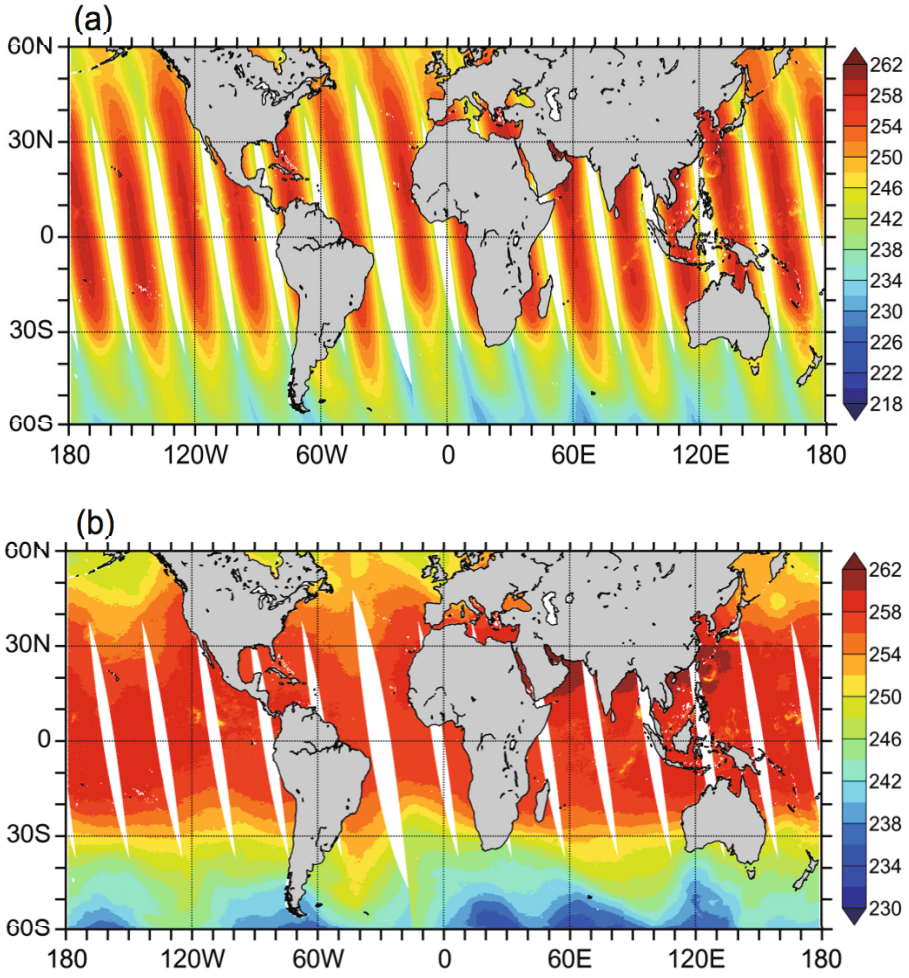

Fig. 2. MWTS-2 channel 4 TBs observed in the ascending node on 7 July 2014 (a) before and (b) after the limb effect adjustment. Units: K.

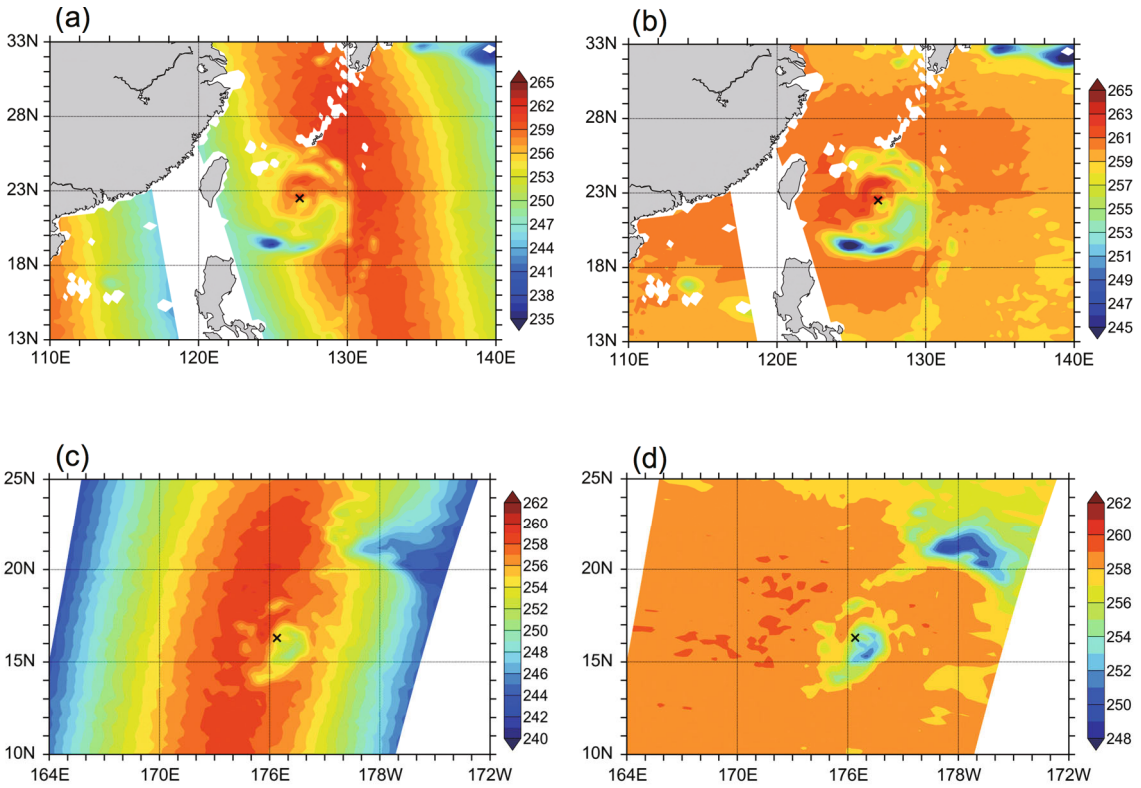

Fig. 3. MWTS-2 channel 4 TBs over areas in the western Pacific Ocean where Typhoons (a, b) Neoguri and (c, d) Genevieve were located. Panels (a) and (b) show the TBs (units: K) observed in the ascending node on 7 July 2014 (a) before and (b) after limb correction. Typhoon Neoguri's center was scanned at 1319 UTC. Panels (c) and (d) are the same as (a) and (b) but for Typhoon Genevieve in the descending node at 2248 UTC 7 August 2014.

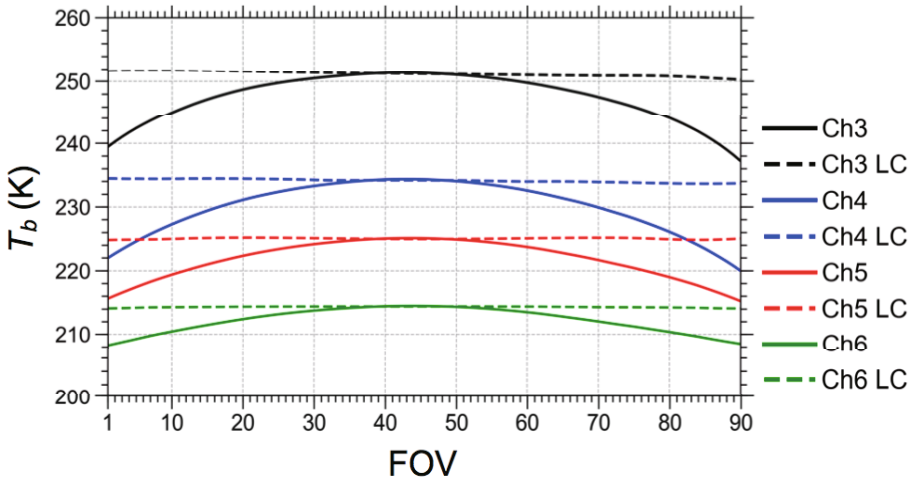

Fig. 4. Mean TBs of channels 3, 4, 5, and 6 before and after limb correction over the period 20–30 August 2014.

its rain bands and clear-sky streaks between (Fig. 3b). The trained coefficients are also applied to observations from Category 4 Typhoon Genevieve (2014; Figs. 3c and d) at 2248 UTC 7 August 2014. The limb correction uncovered weather signals surrounding the storm center from predominant scan variations.

For statistical analysis and validation purposes, Fig. 4 shows 11-day mean TBs from 20–30 August 2014 at channels 3–6 before and after limb correction. Before limb correction, each channel has off-nadir TBs that are cooler than the nadir ones. After limb correction, TBs appear flat at all FOV positions, meaning that TBs at all FOV positions are comparable to those at nadir. To show that LC TBs are more closely and physically related to atmospheric variables, Fig. 5 shows

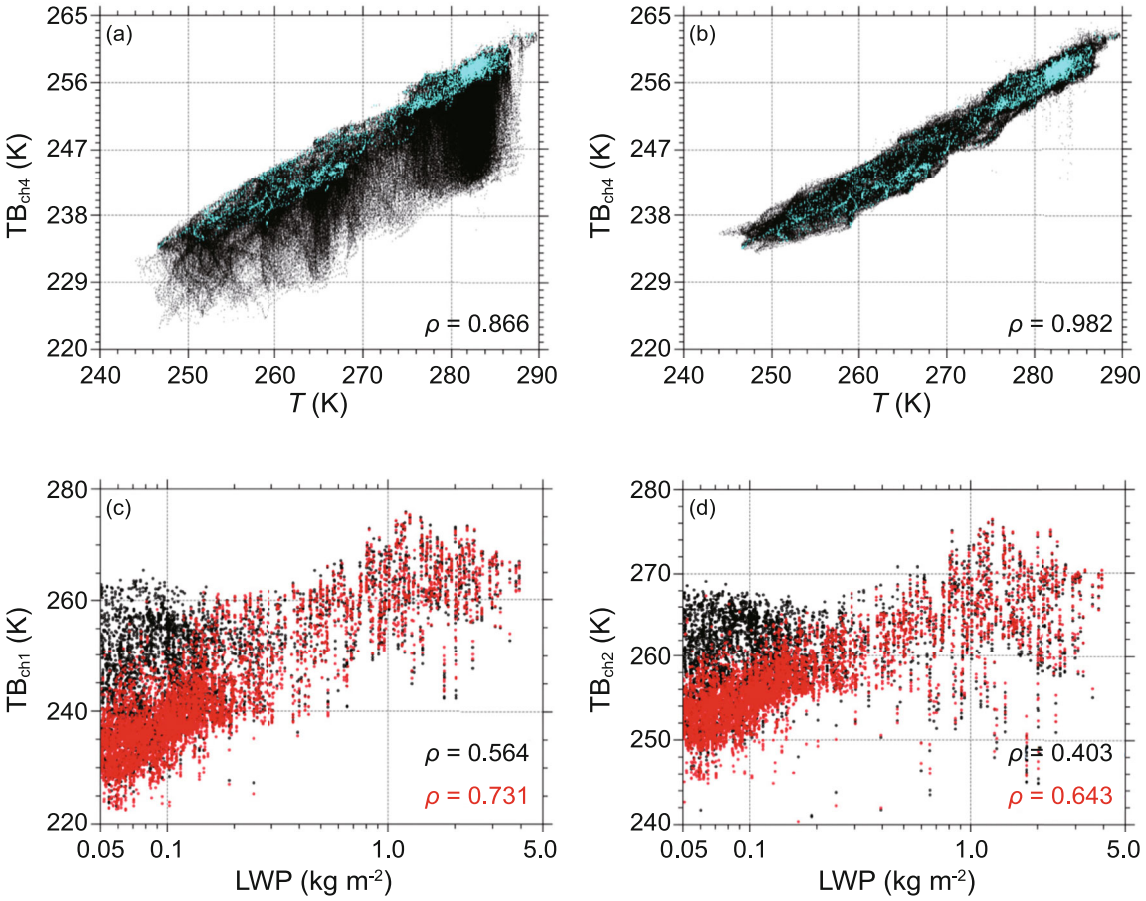

Fig. 5. Channel 4 TBs (a) before and (b) after limb correction as a function of atmospheric temperatures at 700 hPa within the latitude range of 60°S–60°N. Cyan-colored points are observations at nadir FOVs (i.e., FOVs 45 and 46). TBs at channels (c) 1 and (d) 2 with respect to LWP (units: kg m^{-2}) before (black circles) and after (red circles) limb correction. The correlations (ρ) are given in the lower right corner of each panel.

scatterplots of TBs at channel 4 as a function of temperatures at 700 hPa, and TBs at channel 1 as a function of liquid water paths (LWPs). Both physical variables are extracted from the ECMWF reanalysis on the same date and collocated with the MWTS-2 observations. The weighting function of channel 4 peaks at 700 hPa. The atmospheric temperature at this pressure level contributes the most to the radiance observed at channel 4. A strong correlation is thus expected. There is a stronger correlation between TBs and 700-hPa temperatures after limb correction (a correlation coefficient equal to 0.982 as opposed to 0.866 before limb correction; Figs. 5a and b). Similarly, channels 1 and 2 have weighting functions that peak at the surface. Lower tropospheric features such as LWP are expected to influence observed TBs. TBs after limb correction are more strongly correlated with LWP, with correlation coefficients of 0.731 versus 0.564 in channel 1 and 0.643 versus 0.403 in channel 2 (Figs. 5c and d).

4. Summary and conclusions

The MWTS-2 is a cross-track scanning radiometer that samples vertical temperature profiles of the atmosphere from the lower troposphere to the upper stratosphere. Its radiance observations have great potential for applications such as monitoring extreme weather events like typhoons or hurricanes as well as being assimilated into numerical weather prediction models. However, scan-dependent patterns resulting from different scan angles within each scan line dominate radiance measurements.

This study reports a limb correction algorithm for MWTS-2 measurements that mitigates these scan features so that the underlying weather signals can be more evident from TBs. TBs after limb correction expose consistent large-scale weather features both globally and regionally. An example is Typhoon Neoguri, which reached Category 5 on 7 July 2014. LC TBs can reveal detailed storm features. LC TBs are also more closely correlated with atmospheric physical variables such as temperature and LWP.

Acknowledgements. The authors thank the FengYun Satellite Data Center (http://satellite.nsmc.org.cn) for providing the MWTS-2 observational data. The authors also thank the anonymous reviewer(s) for their time and contribution to this study. This study was supported by the National Natural Science Foundation of China (Grant No. 91337218). The algorithms used in this study can be obtained by contacting X. ZOU at xzou1@umd.edu.

REFERENCES

Goldberg, M. D., D. S. Crosby, and L. H. Zhou, 2001: The limb adjustment of AMSU-A observations: Methodology and validation. *J. Appl. Meteor*., **40**(1), 70–83, https://doi.org/10.1175/1520-0450(2001)040<0070:TLAOAA>2.0.CO;2.

Li, J., and G. Q. Liu, 2016: Assimilation of Chinese Fengyun-3B Microwave Temperature Sounder radiances into the Global GRAPES system with an improved cloud detection threshold. *Front. Earth Sci*., **10**(1), 145–158, https://doi.org/10.1007/s11707-015-0499-2.

Li, J., Z. K. Qin, and G. Q. Liu, 2016: A new generation of Chinese FY-3C microwave sounding measurements and the initial assessments of its observations. *Int. J. Remote Sens*., **37**(17), 4035–4058, https://doi.org/10.1080/01431161.2016.1207260.

Tian, X. X., and X. L. Zou, 2016: ATMS- and AMSU-A-derived hurricane warm core structures using a modified retrieval algorithm. *J. Geophys. Res. Atmos*., **121**(21), 12 630–12 646, https://doi.org/10.1002/2016JD025042.

Tian, X. and X. Zou, 2018: Capturing size and intensity changes of hurricanes Irma and Maria (2017) from polar-orbiting satellite microwave radiometers. *J. Atmos. Sci*., **75**, 2509–2522, https://doi.org/10.1175/JAS-D-17-0315.1.

Wang, X., and X. Li, 2014: Preliminary investigation of FengYun-3C microwave temperature sounder (MWTS) measurements. *Remote Sens. Lett*., **5**(12), 1002–1011, https://doi.org/10.1080/2150704X.2014.988305.

Wark, D. Q., 1993: Adjustment of TIROS Operational Vertical Sounder data to a vertical view. NESDIS-64, NOAA, Washington DC, 44 pp.

Zhang, K. X., L. H. Zhou, M. Goldberg, X. P. Liu, W. Wolf, C. Y. Tan, and Q. H. Liu, 2017: A methodology to adjust ATMS observations for limb effect and its applications. *J. Geophys. Res. Atmos*., **122**(21), 11 347–11 356, https://doi.org/10.1002/2017JD026820.

Zou, X., F. Weng, B. Zhang, L. Lin, Z. Qin, and V. Tallapragada, 2013: Impacts of assimilation of ATMS data in HWRF on track and intensity forecasts of 2012 four landfall hurricanes. *J. Geophys. Res. Atmos*., **118**(20), 11 558–11 576, https://doi.org/10.1002/2013JD020405.